Mon. Not. R. Astron. Soc. **000**, 000–000 (0000) Printed 2 February 2008 (MN LaTeX style file v2.2)

arXiv:0712.0859v1 [astro-ph] 6 Dec 2007

Testing the nature of S0 galaxies using planetary nebula kinematics in NGC 1023

E. Noordermeer,[1]* M. R. Merrifield,[1] L. Coccato,[2] M. Arnaboldi,[3] M. Capaccioli,[4] N. G. Douglas,[5] K. C. Freeman,[6] O. Gerhard,[2] K. Kuijken,[7] F. De Lorenzi,[2] N. R. Napolitano[8] and A. J. Romanowsky[9,10]

[1] *University of Nottingham, School of Physics and Astronomy, University Park, NG7 2RD Nottingham, UK*
[2] *Max-Planck-Institut für Extraterrestrische Physik, Giessenbachstrasse, 85741 Garching, Germany*
[3] *European Southern Observatory, Karl-Schwarzschild-Strasse 2, 85748 Garching, Germany*
[4] *Dipartimento di Fisica, Università "Federico II", Naples, Italy*
[5] *Kapteyn Astronomical Institute, University of Groningen, PO Box 800, 9700 AV Groningen, The Netherlands*
[6] *Research School of Astronomy and Astrophysics, Australian National University, Canberra, Australia*
[7] *Leiden Observatory, Leiden University, PO Box 9513, 2300 RA Leiden, The Netherlands*
[8] *Istituto Nazionale di Astrofisica, Osservatorio Astronomico di Capodimonte, Via Moiariello 16, 80131 Naples, Italy*
[9] *UCO/Lick Observatory, University of California, Santa Cruz, CA 95064, USA*
[10] *Departamento de Física, Universidad de Concepción, Casilla 160-C, Concepción, Chile*

accepted for publication in MNRAS; 5-12-2007

ABSTRACT

We investigate the manner in which lenticular galaxies are formed by studying their stellar kinematics: an S0 formed from a fading spiral galaxy should display similar cold outer disc kinematics to its progenitor, while an S0 formed in a minor merger should be more dominated by random motions. In a pilot study to attempt to distinguish between these scenarios, we have measured the planetary nebula (PN) kinematics of the nearby S0 system NGC 1023. Using the Planetary Nebula Spectrograph, we have detected and measured the line-of-sight velocities of 204 candidate PNe in the field of this galaxy. Out to intermediate radii, the system displays the kinematics of a normal rotationally-supported disc system. After correction of its rotational velocities for asymmetric drift, the galaxy lies just below the spiral galaxy Tully–Fisher relation, as one would expect for a fading system. However, at larger radii the kinematics undergo a gradual but major transition to random motion with little rotation. This transition does not seem to reflect a change in the viewing geometry or the presence of a distinct halo component, since the number counts of PNe follow the same simple exponential decline as the stellar continuum with the same projected disc ellipticity out to large radii. The galaxy's small companion, NGC 1023A, does not seem to be large enough to have caused the observed modification either. This combination of properties would seem to indicate a complex evolutionary history in either the transition to form an S0 or in the past life of the spiral galaxy from which the S0 formed. More data sets of this type from both spirals and S0s are needed in order to definitively determine the relationship between these types of system.

Key words: galaxies: individual: NGC 1023 – galaxies: individual: NGC 1023A – galaxies: elliptical and lenticular, cD – galaxies: structure – galaxies: kinematics and dynamics – galaxies: evolution

1 INTRODUCTION

Lenticular, or S0, galaxies make up about 25% of all large galaxies in the local Universe (Dressler 1980). Their location in Hubble's (1926) tuning fork diagram at the apex between ellipticals and spirals emphasizes their importance in understanding galaxy evolution, yet even the most basic question of whether they are more closely related to the spiral systems on their right or the ellipticals on their left remains unanswered. In the nearby Universe, S0s are more prevalent in galaxy clusters than in the field, at the expense of a smaller fraction of spirals (Dressler 1980). At higher redshifts, however, the S0 fraction in clusters is smaller, and the spiral fraction correspondingly larger (Dressler et al. 1997; Couch et al. 1998), suggesting that the latter are the progenitors of the lenticular galaxies observed in the present-day Universe. How this transformation comes about, however, is still unclear. On the one hand, it is possible that S0s form when spiral galaxies lose their gas through interactions with the intergalactic medium and thus simply stop forming stars (Quilis et al. 2000). On the other, S0s could form from mergers: while equal-mass mergers produce elliptical galaxies, the equivalent unequal-mass mergers result in hybrid systems with both spheroidal and disc-like components, which have lost most of their gas through starbursts and tidal tails (Bekki 1998; Bournaud et al. 2004, 2005).

---

* email:edo.noordermeer@nottingham.ac.uk

Distinguishing between these two scenarios is not straightforward. In principle, deep photometry of lenticulars should hold clues: in the merger scenario, the central bulge extends outward into a diffuse stellar halo, such that the light in the outer regions originates mainly from a spheroidal component and the disc only dominates at intermediate radii. Indeed, a simple outward extrapolation of the bulge intensity profiles of S0s seems to imply that this component often wins out at large radii, with the disc only ever being important at intermediate radii (Seifert & Scorza 1996). However, this behaviour depends on the fitting functions and decomposition methods adopted, how the sky background is flatfielded and subtracted, etc.; different choices for these factors can give equally good fits, but with the disc dominant out to the largest radii (Laurikainen et al. 2005), as the gas stripping scenario predicts. It thus seems unlikely that photometry alone will answer the question.

It is therefore perhaps more promising to look at the dynamics of these systems, which may offer a clearer record of their life histories. If lenticulars are simply gas-stripped or quenched spirals, then one would expect their stellar dynamics to be only modestly affected by the transition. The gas stripping process may cause a final flickering of star formation in the disc of the galaxy (Quilis et al. 2000), and a modest degree of secular evolution is needed to explain the larger bulge-to-disc ratio in lenticulars compared to spiral galaxies (Christlein & Zabludoff (2004), although this result seems to be contradicted by the results from Laurikainen et al. (2005)). However, such effects are expected to play a rôle mainly in the central parts of the galaxies. At large radii, the galaxies should largely keep the disc-like kinematics of a spiral, with rotation dominating over random motions. On the other hand, if S0s are formed through mergers, simulations show that the resulting systems are much 'hotter', with velocity dispersions in the outer regions as large as the rotational velocities (Bournaud et al. 2004, 2005). In addition, the dynamics provide a measure of the mass distribution in these systems, allowing us to explore the scaling relations between mass and luminosity. Thus, for example, we can see if lenticulars follow a similar Tully–Fisher relation to normal spiral galaxies, as one might expect if the S0s are their descendants.

Unfortunately, results from previous dynamical studies have proved somewhat inconclusive. For example, Mathieu et al. (2002) found that S0 galaxies obey a tight Tully–Fisher relation, but offset to fainter magnitudes from the relation for spiral galaxies, suggesting that S0s are formed from spirals that faded when they ceased forming new stars. However, this result conflicts with the analysis of Neistein et al. (1999), who found a huge scatter in the luminosity versus rotation speed relation for S0s and, instead, found that the central stellar velocity dispersion is a better predictor for the luminosity via the fundamental plane relations, suggesting that S0s are more closely related to ellipticals. More recently, Bedregal et al. (2006) obtained much deeper absorption-line spectroscopy, which made the determination of the rotation curve more reliable, and found a relation between the offset from the spiral galaxy Tully–Fisher relation and the age of S0s' stellar populations in the manner expected if S0s are passively fading away from their former lives as spirals.

However, even deep absorption-line spectroscopy is limited to the brighter inner parts of S0 galaxies. This limitation is unfortunate, as much of the most useful dynamical information resides in the outer parts of the system. The Tully–Fisher analysis, for example, relies on getting out to large enough radii to determine the asymptotic form of the rotation curve, and failure to do so can result in significant biases in the results (Noordermeer & Verheijen 2007). In addition, the longer dynamical timescales at larger radii means that any evidence as to a system's life history will likely be better preserved at these radii.

Fortunately, an alternative probe of stellar kinematics exists that can operate at even the faintest surface brightness levels. Planetary nebulae (PNe) are simply low mass stars at the ends of their lives, so their kinematics should faithfully trace the bulk stellar dynamics. In addition, their strong emission features, particularly the 5007Å [OIII] line, means that they can be reliably identified and their kinematics readily measured. To exploit this resource, a specialized instrument, the Planetary Nebula Spectrograph (PN.S), has been constructed. Mounted at the 4.2m William Herschel Telescope[1], the PN.S is designed to identify PNe and measure their locations and velocities in a single observation; details of the instrument and its operation can be found in Douglas et al. (2002).

As a first test of the use of this instrument to understand the nature of lenticular galaxies, we obtained an observation of the typical S0 system NGC 1023. This object is the brightest of a group of 13 galaxies (Tully 1980), and, as one of the nearest large lenticular galaxies at a distance of 11.4 Mpc (Tonry et al. 2001), it offers an obvious first target. It also has a companion, NGC 1023A, near the eastern edge of its disc at a projected distance of 9 kpc (Barbon & Capaccioli 1975). Based on the peculiar structure of neutral gas in the area it has been suggested that these systems are closely interacting or even merging (Sancisi et al. 1984; Capaccioli et al. 1986). However, after a careful analysis of an optical image of the NGC 1023/1023A system, we show below that the companion is most likely too small to cause significant disruptions in the dynamical state of the main galaxy. Thus, the presence of the companion is probably of little influence for the interpretation of the kinematical data we obtained.

---

[1] The William Herschel and Isaac Newton Telescopes are operated on the island of La Palma by the Isaac Newton Group in the Spanish Observatorio del Roque de los Muchachos of the Instituto de Astrofisica de Canarias.

Table 1. PN.S observations of NGC 1023.

date	exposure time		seeing	photometric?
	West	East		
	s	s	$''$	
23/10/2006	7200	7200	1.0	yes
27/10/2006	5400	3600	1.4	no

Absorption line spectroscopy for NGC 1023 has been presented by various groups (Simien & Prugniel 1997; Neistein et al. 1999; Debattista et al. 2002; Emsellem et al. 2004) and clearly shows that the galaxy is rotating regularly. However, these data underline the limitations of such conventional techniques, since they reach to a maximum radius of only 100$''$, barely outside the area dominated by the central bulge. They thus do not probe the regions likely to discriminate between the various scenarios for S0 formation. As we shall see below, the PN.S data reach to approximately four times this radius, well into the disc-dominated region and beyond.

The remainder of this paper is structured as follows. In Section 2 we present the observations and describe the basic data reduction. In Section 3, we discuss the spatial and velocity distribution of the detected PNe, and present the method adopted to disentangle the objects belonging to NGC 1023 from those in NGC 1023A. Section 4 explores the dynamics of the main galaxy in more detail, derives the radial profiles of rotation velocity and velocity dispersion, and places NGC 1023 on the Tully–Fisher relation. Finally, in Section 5, we discuss the implications of our results.

2 OBSERVATIONS AND DATA REDUCTION

2.1 Planetary nebula data

NGC 1023 was observed with the Planetary Nebula Spectrograph for a total of 6.5 hours on the nights of 2006 October 23 and 27. The galaxy is too large to fit within the 10$'$ PN.S field of view, so the observation was split between two pointings ("West" and "East") along the major axis of the galaxy, overlapped by about 4$'$. Table 1 provides a summary of the integration time and seeing. All exposures were made through the 'AB' filter, which has a central wavelength of 5026Å and a FWHM bandpass of 44Å. This wavelength coverage provides a velocity window for the detection of PNe of -168 – 2467 $\mathrm{km\,s^{-1}}$, wide enough to detect all PNe which are physically bound to NGC 1023, which has a systemic velocity of $\sim 600\,\mathrm{km\,s^{-1}}$ (see below).

The data reduction followed the standard PN.S pipeline described in detail in Douglas et al. (2007). The only further enhancement to the reduction involved the development of a procedure to help measure the positions of PNe that were confused with the short continuum spectra of stars in the spectrograph's field: by reflecting these "star trails" about their centres in the undispersed direction, it proved possible to subtract out the contribution of the stellar spectrum, leaving just the point-like emission line from the PN.

The observations for the East and West pointings were reduced separately, and PN locations and velocities were derived independently from each pointing. Since the two pointings overlapped in the central regions of the galaxy, a significant number of objects were detected in both, and the differences in their positions, velocities and magnitudes provide a useful internal check on the robustness of the instrument and the pipeline reduction. The positions, velocities and instrumental magnitudes for the 116 objects found in both pointings have mean differences of 0.17$''$, 1.8 $\mathrm{km\,s^{-1}}$ and 0.05 mag, with an RMS scatter of 0.22$''$, 16.3 $\mathrm{km\,s^{-1}}$ and 0.15 mag respectively. These errors are within the design tolerance of the instrument: given the large spatial and velocity scales of the structure under study, they will have no significant impact on this dynamical study of NGC 1023.

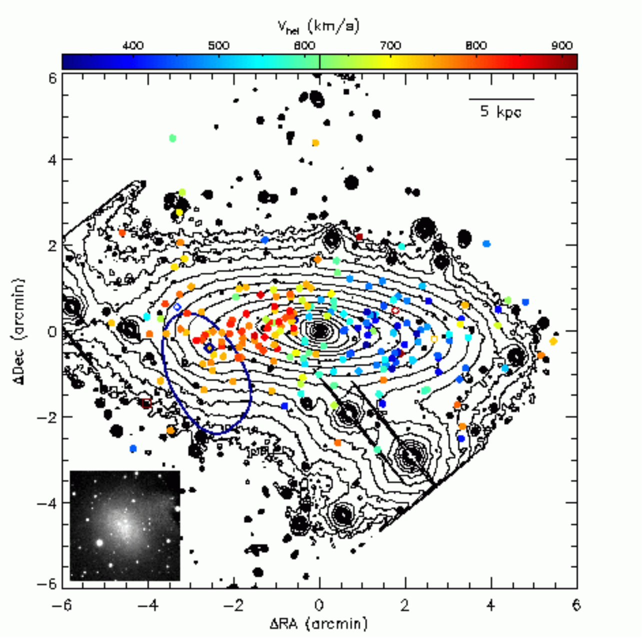

Figure 1. The distribution of stellar light and planetary nebula in NGC 1023. Black contours show R-band isophotes, ranging from 14.5 to 25.5 $\mathrm{mag\,arcsec^{-2}}$, in steps of 0.5 $\mathrm{mag\,arcsec^{-2}}$. The solid bullets show the positions of the PNe, with the colours indicating the heliocentric velocities. Open circles indicate the $> 3\sigma$-outliers from the tilted-ring analysis; the square symbol indicates the object which deviates more than 1000 $\mathrm{km\,s^{-1}}$ from the systemic velocity of the galaxy. The blue contour indicates the region where PNe are more likely to belong to the dwarf companion galaxy NGC 1023A than to the main galaxy; the centre of the companion is indicated with the blue diamond. The 20 PNe in this region were removed from the kinematic analysis. The inset shows a grayscale image of NGC 1023A, at the same scale as the main figure, created from the original image by subtracting a model of NGC 1023 (see text for details). The excess light on its western side is a result of imperfect subtraction of the main galaxy.

In addition to the 116 objects detected in both pointings, 88 objects were found in the individual pointings in the western and eastern outskirts of the galaxy. The resulting final catalogue of 204 objects is presented in Table 2.

2.2 Imaging data

We have supplemented the PN data with R- and B-band images obtained with the Isaac Newton Telescope on 1995 December 25, using the Prime Focus Camera. The 300 second exposures were flatfielded and flux calibrated in the conventional manner. A contour plot of the resulting R-band

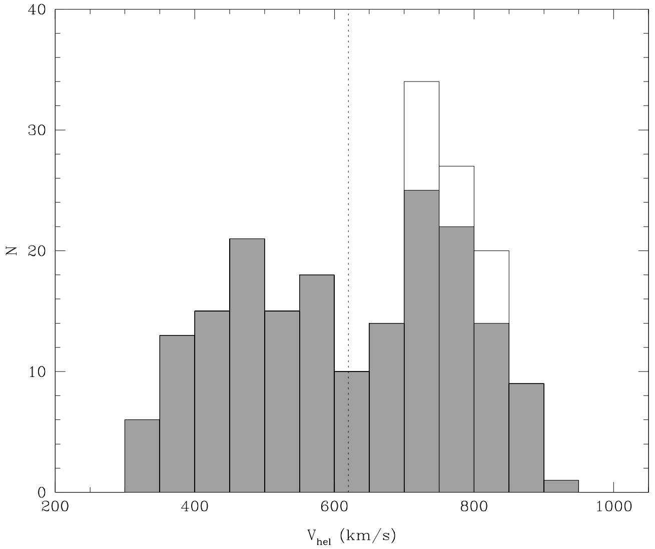

Figure 2. The velocity distribution of the PNe system of NGC 1023. The grey histogram indicates the PNe in the main galaxy, whereas the white regions show the PNe which were assigned to the companion. The dotted line indicates the systemic velocity.

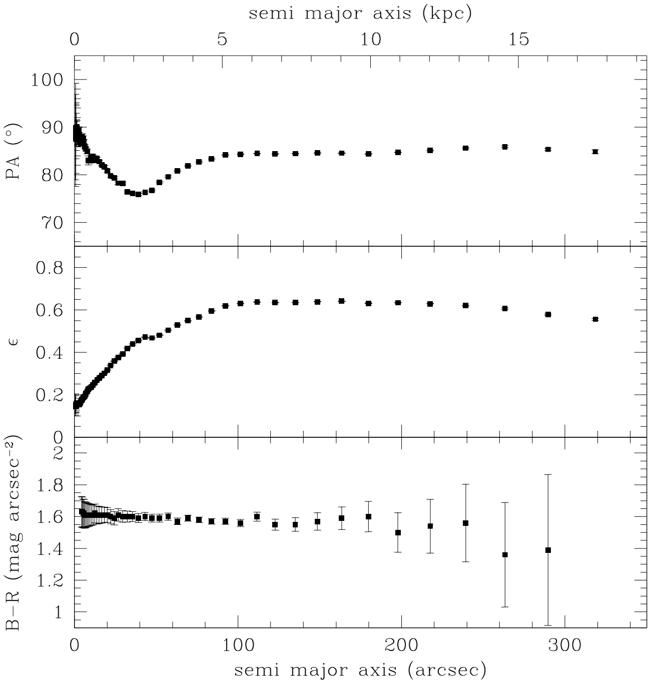

Figure 3. Results from the isophotal analysis of NGC 1023. The top and middle panels show the fitted position angle (north through east) and ellipticity of the isophotes respectively. The bottom panel shows the B-R colour.

image is shown in Figure 1, together with a colour coded representation of the PN velocity field.

3 THE PLANETARY NEBULA SYSTEM OF NGC 1023

Figure 1 shows that the PN distribution generally follows the optical image, except for the inner regions where the bright continuum background inhibits the detection of PNe (cf. Douglas et al. 2007). Note that a significant number of objects are detected out to the very faintest measured optical isophotes. One such object (ID 200, marked with the open square in Figure 1) has a highly discrepant velocity ($V_{\rm hel} = 1703\,{\rm km\,s^{-1}}$), and is probably an unrelated background source. This object has accordingly been excluded from the dynamical analysis.

The velocity distribution of the remaining objects is shown in Figure 2. The distribution shows a clear asymmetry, with an excess of objects around $V_{\rm hel} = 750\,{\rm km\,s^{-1}}$. This value coincides with the measured velocity for the dwarf companion NGC 1023A ($742 \pm 30{\rm km\,s^{-1}}$; Capaccioli et al. 1986) and, indeed, inspection of Figure 1 reveals a concentration of objects near this velocity in the region where the isophotes show the distorted signature of contamination by this object. Inconveniently, the rotation of NGC 1023 is such that one cannot cleanly separate the two galaxies on the basis of their kinematics, since the mean velocities of the systems are very similar in this region. We therefore adopt the procedure developed by Douglas et al. (2007) to assign membership based on local relative surface brightness contributions.

We first study the optical morphology of NGC 1023 by masking out all foreground stars, as well as the region contaminated by NGC 1023A, and fitting elliptical isophotes to the remaining parts of the image. The results from this procedure are shown in the top and middle panel of Figure 3 and show that, after the exclusion of the companion, NGC 1023 has a highly regular structure. In particular, the position angle and ellipticity of the galaxy are remarkably constant outside the bulge-dominated area and do not show any signs of deviation from a simple, flat disc out to the outermost radii. Note that the colour of the fitted isophotes is also constant with radius within the errors (bottom panel in Figure 3). Based on the fitted isophotes and the derived intensity profile (see Figure 4), we created a model image for NGC 1023, interpolating over the masked regions. This model image was then subtracted from the original, leaving the emission from NGC 1023A in the residual image. A grayscale representation of its intensity distribution is shown in the inset in Figure 1. Note that the companion is very small compared to NGC 1023 itself, with an R-band main-to-companion luminosity ratio of about 40:1.

We then followed the same method to create a model image for NGC 1023A, and divided the two model images to calculate the ratio of flux from the two galaxies at each location in the field, and hence to which system a PN at that position is most likely to belong. The only additional complication is that we need to take into account the fact that NGC 1023A has a bluer colour than NGC 1023, which increases the specific frequency of PNe. Having allowed for this effect using the relations between colour and specific frequency from Hui et al. (1993), we can construct the contour at which a PN is equally likely to be a member of either system, as shown in Figure 1.

As the simplest approach to assigning membership, we associate the 20 PNe in this region with NGC 1023A, leaving 183 PNe in the final NGC 1023 catalogue. As Figure 2 shows, the 20 PNe associated with NGC 1023A have a narrow velocity distribution with a full width of 130 $\mathrm{km\,s^{-1}}$, centered around a median velocity of 767 $\mathrm{km\,s^{-1}}$. The overall velocity distribution of the 183 remaining objects is symmetric and has the two-horned structure characteristic of a rotating system. Clearly, the simple spatial cut applied here will result in some modest level of misidentification, but experiments that excluded or included more objects showed that the following results are not sensitive to this residual contamination. Furthermore, measurements of the average streaming velocities and velocity dispersions on the approaching and receding halves of the galaxy separately show that, after the exclusion of the NGC 1023A PNe, both sides are consistent within the errorbars.

In Figure 4, we compare the NGC 1023 PN number densities with the R-band photometric profile. Outside a radius of about 100″, the PN number counts follow a similar exponential distribution to the stellar light. This good match lends support to the assumption that the PNe are an unbiased tracer of the dominant stellar components in such an old disc population (see also Douglas et al. 2007). At smaller radii, the PN counts become incomplete due to the difficulty of detecting them against the brighter parts of the galaxy. Given the nature of source detection in a slitless spectrograph like the PN.S, there is also potential for kinematic as well as photometric selection biases at the smallest radii where the luminosity gradients are strongest (Douglas et al. 2007), so we do not use the PN kinematics in this region, instead basing our dynamical analysis on the complementary absorption-line data that are available at these higher surface brightnesses. However, at larger radii the completeness of the PN data means that we can reliably use our measurements to study stellar kinematics all the way out to an equivalent R-band surface brightness of about 28 $\mathrm{mag\,arcsec^{-2}}$, or 8 disc scale lengths, a region completely inaccessible to the conventional absorption-line analysis.

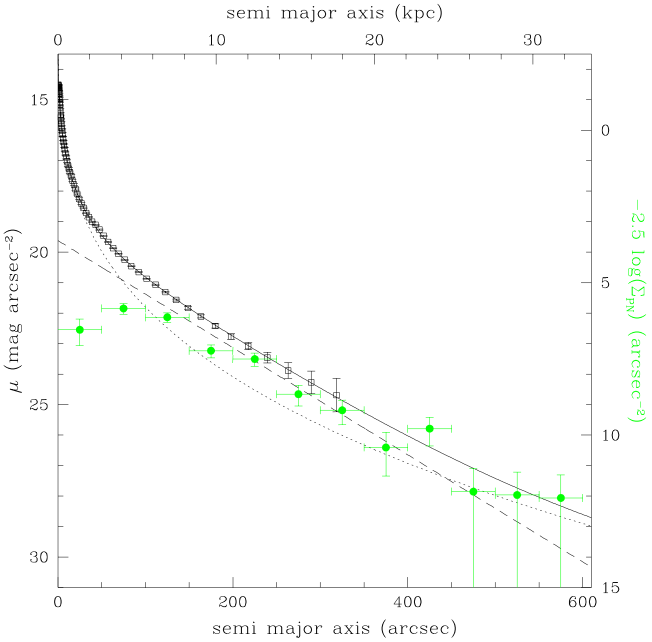

Figure 4. Comparison of the radial PN density distribution in NGC 1023 (green filled circles) with the R-band photometric profile (black open squares). Both were measured on concentric ellipses with an ellipticity of 0.63 and a position angle of 85°. Dotted and dashed lines indicate Sérsic bulge and exponential disc profiles fitted to the R-band profile and the solid line shows the sum of the two components. The fitted bulge and disc have an effective radius and exponential scale length of 32 and 62″ (1.8 and 3.4 kpc) respectively, which are typical values for a lenticular galaxy of this luminosity (Barway et al. 2007).

4 KINEMATIC ANALYSIS

4.1 Rotational velocities and velocity dispersions

To study the kinematic structure of NGC 1023, we first use a discrete tilted ring analysis, which is in essence the equivalent for discrete sources of the familiar tilted-ring method used for 2D gas velocity fields (Begeman 1987; Begeman 1989). The sample of 183 PNe in NGC 1023 was divided into 11 radial bins, and the velocities in each bin were fitted with a function of the form

$$V_{\mathrm{obs}} = V_{\mathrm{sys}} + V_{\mathrm{rot}} \sin(i) \cos(\theta), \qquad (1)$$

where θ is the azimuthal angle in the plane of the galaxy, starting from the receding side on the major axis. We assumed that the disc of NGC 1023 has an inclination with respect to the line of sight of $i = 71.5^\circ$ (based on the ellipticity of the optical isophotes and an assumed intrinsic thickness of the disc of 0.2) and a position angle of $PA = 85^\circ$ from north. We have tested the sensitivity of our results to the assumed values for the orientation angles by doing additional fits with inclinations ranging from 65 to 75°, but found that the effects on the fitted velocities and velocity dispersions (see below) were modest and did not affect our results significantly. The uncertainties in PA have negligible effect on the kinematic measurements.

In the first instance, we let the systemic velocity V_{sys} vary freely from ring to ring. The values found from that fit were then averaged to find a mean of 617 $\mathrm{km\,s^{-1}}$, which was subsequently fixed as the global systemic velocity for the entire galaxy. In order to account for the possibility of contamination by unrelated objects such as background galaxies, a simple 3 sigma-clipping criterion was applied to exclude outliers from the fit; the 3 PNe with discrepant velocities which we identified in this manner are indicated with the open symbols in Figure 1. The final resulting mean streaming velocity as a function of ring radius is shown in the upper panel of Figure 5.

In addition to the rotational velocities of the PNe in each ring, we also measure the residual velocities around the fits. These residuals constrain the velocity dispersions along the principal axes of the system, with the measured line-of-sight dispersion at a given location in the disc given by:

$$\sigma_{\mathrm{los}}^2 = \sigma_R^2 \sin^2 i \sin^2\theta + \sigma_\phi^2 \sin^2 i \cos^2\theta + \sigma_z^2 \cos^2 i, \qquad (2)$$

where σ_R, σ_ϕ and σ_z are the components of dispersion along the cylindrical polar axes. NGC 1023 is sufficiently close to edge-on and the z-component of random velocity sufficiently small that σ_z makes a negligible contribution to the observed dispersion. In principle, the remaining two components can be disentangled by measuring σ_{los} as a function of azimuth. However, with only $\sim$ 20 PNe per radial bin, there is not enough signal to derive these components individually. Instead, we solve for a single component under the assumption

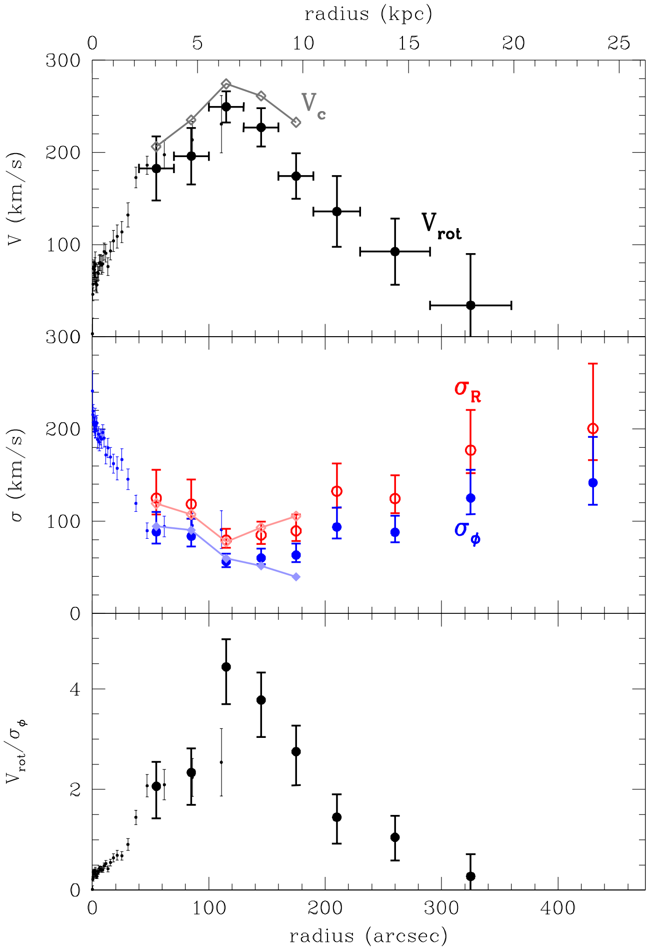

Figure 5. Results from the kinematical analysis. The upper panel shows the mean streaming analysis. Small data points with errorbars are from the major-axis absorption-line data of Debattista et al. (2002). Large filled data points are from the tilted ring analysis of the PNe velocities; the errorbars indicate the formal fitting uncertainties. The connected grey diamonds show the rotation curve after iterative correction for asymmetric drift (see text for details). The middle panel shows the analysis of random motions. Small data points with errors are once again major-axis absorption-line data from Debattista et al. (2002). The open red symbols and large filled blue symbols are the radial and tangential components of velocity dispersion respectively, as inferred from the tilted-ring fit to the PNe data; the errorbars show, again, the formal errors. The connected diamonds show the corresponding values after the iterative correction for asymmetric drift. The bottom panel shows the ratio between rotational motion and the azimuthal component of the velocity dispersion.

that the other component is coupled to it via the epicyclic approximation,

$$\frac{\sigma_\phi^2}{\sigma_R^2} = \frac{1}{2}\left(1 + \frac{d(\ln V_c)}{d(\ln R)}\right). \qquad (3)$$

(Binney & Tremaine 1987). Clearly, this approximation breaks down if the random velocities become too large, but it offers a useful model for starting to understand the dynamics of the disc-dominated parts of this system.

There is one further complication in that the circular speed, V_c, for this system is not known since the observed rotation speed of the stars is lowered due to asymmetric drift (see Section 4.2). However, as a first approximation it is probably not too unreasonable to assume a flat rotation curve outside the very central regions, so that the derivative in equation 3 vanishes at the radii of the PNe and $\sigma_R/\sigma_\phi = \sqrt{2}$. With this enforced coupling, we obtain the velocity dispersion profiles for the individual components shown as data points in the middle panel of Figure 5.

Several points are immediately apparent from even this approximate analysis. First, it is clear that the kinematics inferred from the PNe match up very well to those inferred from the absorption line data of Debattista et al. (2002), also shown in Figure 5. This match further confirms that the two types of data sample the same underlying kinematic tracer and underlines the complementarity between the data sets, with the PNe taking over at just the point where the absorption-line data give out. Second, it is immediately clear that the absorption-line data do not tell the full story with this galaxy, as out to the largest radius that they trace one obtains a picture of a well-behaved system with monotonically declining dispersion profiles and rising rotation profile. However, at the much larger radii traced by the PNe these trends unexpectedly reverse entirely, and the velocity dispersions increase rapidly at the expense of a sharply dropping rotational velocity profile. As a result, the PN system becomes dominated again by random motions outside a radius of about 250″(14 kpc), with rotation only being dominant at intermediate radii (between 1.7 and 13 kpc).

Before continuing our analysis, we must ask the question whether geometric effects can explain this peculiar behaviour. If the outer disc were significantly flared or warped towards edge-on, the line of sight would sample a large range of radii, effectively lowering the measured $V_{\rm rot}$ and increasing σ_ϕ. Although the regularity of the outer isophotes of NGC 1023 (see Figure 3) seems to argue against such effects, we have nevertheless carried out simple simulations to study the effects of thickened discs and varying viewing angles on the observed velocity distributions. We have found that, although line-of-sight integration effects can indeed increase the velocity dispersions, the effect is always at least an order of magnitude smaller than the velocity amplitude of the rotation curve. We have not been able to reproduce the observed velocity dispersions other than by assuming that they are intrinsic. Furthermore, although the line-of-sight integration effects did indeed lower the mean streaming velocities along the major axis of the system, the mean velocities were often increased at other position angles, such that the azimuthally averaged rotation velocity remained largely unchanged.

As a final check, we show in Figure 6 the velocities of individual PNe within 20° of the major and minor axes of NGC 1023. The increase in velocity dispersion with radius and the associated decrease in average streaming motion along the major axis are clearly visible. Note in particular the counter-rotating PNe on both sides of the major axis; such objects would not exist in a flared or warped, but otherwise regularly rotating, disc.

4.2 Asymmetric drift and the circular velocity curve

To proceed further with our analysis, for example to study the location of NGC 1023 on the Tully–Fisher relation, we

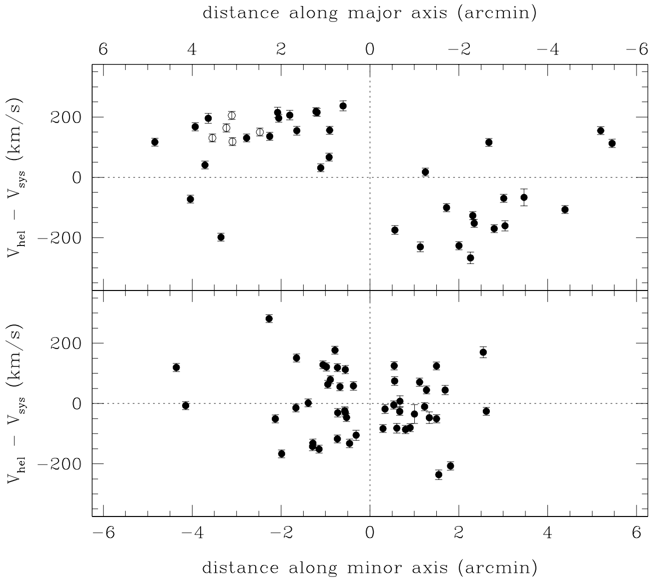

Figure 6. PNe position-velocity diagrams along the major (top panel) and minor (bottom) axes. Each panel shows the velocities of all objects that lie within 20° in θ of the respective axes. Open symbols indicate PNe in the region contaminated by NGC 1023A (i.e. objects inside the blue contour in Figure 1).

must derive the rotation curve. To do so, we must correct the measured mean rotation of the stellar component for asymmetric drift via the equation

$$V_c^2 = V_{\rm rot}^2 + \sigma_\phi^2 - \sigma_R^2\left(1+\frac{d(\ln\nu)}{d(\ln R)}\right) - R\frac{d\sigma_R^2}{dR}, \qquad (4)$$

where we have assumed that the tilt term, $d(\overline{V_R V_z})/dz$, is negligible (Binney & Tremaine 1987). This equation is only valid when the motions are dominated by rotation and cannot be applied to systems dominated by random motions, so we only apply it to the points at intermediate radii ($40'' < R < 200''$) where the mean streaming motions exceed the random velocities (see Figure 5). At these radii, the density of the kinematic tracer, $\nu(r)$, is well described by a simple exponential with scale-length $h = 62''$ (see Figure 4), so we adopt that functional form for this analysis.

Now, we have three coupled equations, 2 – 4, for the three unknowns, V_c, σ_ϕ and σ_R, which we can solve in an iterative fashion. Starting with the data points from Figure 5, we use equation 4 to obtain an estimate for V_c. This rotation curve is then used to re-evaluate the ratio between the azimuthal and radial velocity dispersions via equation 3 and new dispersion profiles are calculated, which in turn are used to refine the estimate for the rotation curve. This process converges rapidly, and results in the final dispersion profiles and rotation curve shown connected by solid lines in Figure 5.

It is apparent that the refinement of the rotation curve does not have much impact on the inferred shape of the velocity ellipsoid, beyond a stretching of its shape in the radial direction at large radii. The correction for asymmetric drift does, however, result in a significant difference between the mean streaming speed and the inferred rotation curve. While the mean streaming velocity was found to drop faster than a Keplerian decline, the rotation curve drops more slowly, as is physically required. Indeed, between 100 and 200″, the variation in circular speed with radius is relatively modest and, given the large errorbars on the original uncorrected data points, the rotation curve is consistent with being flat.

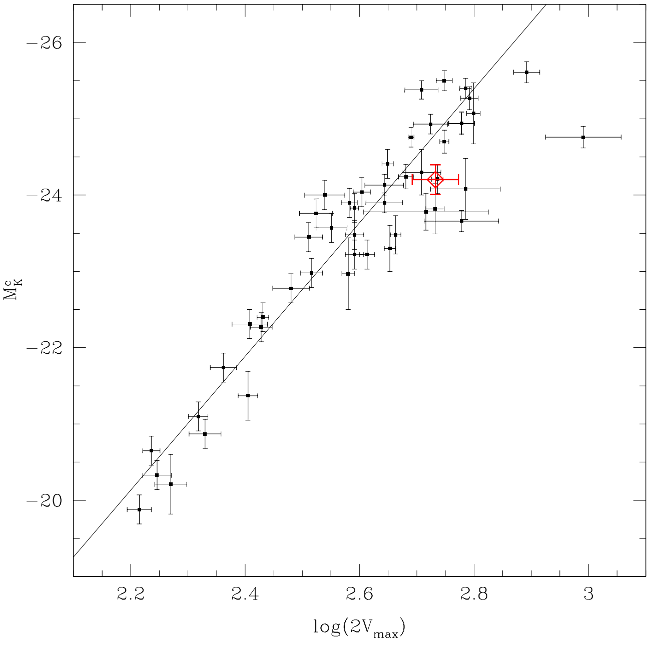

Figure 7. The location of NGC 1023 on the K-band Tully–Fisher relation. Small black data points show the Tully–Fisher relation from Noordermeer & Verheijen (2007), with the solid line showing the best linear fit. The location of NGC 1023 is indicated with the large red diamond.

4.3 The location of NGC 1023 on the Tully-Fisher relation

From the rotation curve shown in Figure 5, we estimate a maximum circular speed of $V_{\rm c,max} = 270 \pm 25\,{\rm km\,s^{-1}}$, which we use to place NGC 1023 on the K-band Tully–Fisher relation. For its luminosity, we adopt the total apparent magnitude as measured by 2MASS[2], and follow the same conversions as in Noordermeer & Verheijen (2007) to derive the absolute magnitude. This figure is marginally inflated since the 2MASS data have not subtracted out the contribution from NGC 1023A. However, from the R-band image in Figure 1, we know that this contribution is at most 0.02 magnitudes, which is not large enough to cause any significant shift. Using these values, we place NGC 1023 on the Tully–Fisher relation shown in Figure 7.

It is clear from this figure that NGC 1023's location is entirely consistent with what one would expect for a normal disc galaxy: its offset below the mean relation (≈ −0.6 mag) is only 1.5 times the scatter as measured by Noordermeer & Verheijen (2007) and the uncertainties in $V_{c,max}$ can account for most of this offset. The offset can, alternatively, also be explained if NGC 1023 formed from a normal star-forming spiral galaxy about 1 Gyr ago, and has been fading passively since (Bedregal et al. 2006).

---

[2] 2MASS (http://www.ipac.caltech.edu/2mass/) is a joint project of the University of Massachusetts and the Infrared Processing and Analysis Center/California Institute of Technology, funded by the National Aeronautics and Space Administration and the National Science Foundation.

5 DISCUSSION AND CONCLUSIONS

In this paper, we have set out to show that dynamical studies of the planetary nebulae in S0 galaxies can shed some light on the origins of these systems through a pilot study of the archetypal lenticular system NGC 1023. However, as so often in astronomy, the picture that emerges from these data is somewhat complex.

At small radii, the absorption-line spectra show a well-behaved dynamical structure typical of a system that is bulge-dominated (i.e. kinematically 'hot') at its centre, with a transition to rotation-dominated disc kinematics at larger radii. This picture is confirmed and extended by the PN data to a reasonably flat maximum in the rotation curve and a continuing decline in the velocity dispersions. Combining these data with the K-band luminosity places NGC 1023 a little below the mean Tully–Fisher relation for spiral galaxies, as one would expect for a passively fading stellar population. The data in these regions fit very nicely with a picture in which this galaxy evolved from a normal spiral system that shut down its star formation after losing its gas.

The largest radii probed by the PNe uncover a completely different story and contradict the 'fading spiral' hypothesis. Outside four disc scale-lengths, the kinematics become completely dominated by random motions. Having excluded the possibility that this behaviour is caused by a change in viewing geometry (e.g. a strongly warped or flared disc), this change suggests that we are seeing a transition from a disc population to the kind of hot stellar halo that might be produced by a minor merger. If such a merger stripped the gas from the galaxy, it would have caused the end of star formation as well and the subsequent fading of the stellar population would again be consistent with the observed offset from the mean Tully-Fisher relation. There are, however, no signs of any accompanying change in the photometry at these radii, as both the stellar light and PN number counts seem to be well reproduced by a single exponential profile (see Figure 4). There is little indication either of the continuum image or PN distribution becoming rounder at the transition radius; instead, the outer isophotes appear as elongated as the ones at intermediate radii (see Figure 3). Moreover, the observed dynamical structure seems to be inconsistent with what is predicted in the minor merger simulations. Mergers with the mass ratios required to transform a spiral galaxy into a lenticular (5:1 – 10:1, Bournaud et al. 2005) appear to affect the dynamical structure of the remnant at all radii, such that they are not rotationally-dominated anywhere. In particular, they do not reproduce the region with $V_{\rm rot}/\sigma_R > 3$ observed at intermediate radii in NGC 1023. Furthermore, the simulations predict a flat, or slowly declining, velocity dispersion profile in the outer regions, in contrast with the observed sharp increase in the case of NGC 1023. Note that mergers between spirals and ellipticals do not reproduce the peculiar kinematics of NGC 1023 either (e.g. Di Matteo et al. 2007).

So, to sum up, the fading spiral scenario fits with the properties of NGC 1023 at small radii but fails to explain its strange kinematic structure at large radii, while the minor merger scenario fits better with the data at large radii but fails to explain the presence of a rotation-dominated disc at small radii.

One possibility is that the disturbed kinematics reflect an ongoing interaction with NGC 1023A, but this seems rather unlikely. As the companion is somewhat bluer than the main galaxy, the stellar mass ratio of main-to-companion galaxy is likely to be more extreme than the R-band luminosity ratio, which at 40:1 is already large. Even though NGC 1023A may be dark matter dominated, it seems implausible on energetic grounds that such a minor merger could have such a profound influence on the main galaxy's kinematics. Simulations of minor mergers show that they can heat up galactic discs and produce, in some cases, velocity dispersions up to 100 $\mathrm{km\,s^{-1}}$ (Bournaud et al. 2004), but this requires mass ratios as small as 10:1 or even 5:1. Mergers with smaller satellites increase the velocity dispersions by at most a few tens of $\mathrm{km\,s^{-1}}$ (Quinn et al. 1993; Velázquez & White 1999), in stark contrast with the dispersions in the outer parts of NGC 1023 ($\approx 200\ \mathrm{km\,s^{-1}}$). Moreover, the fact that the optical morphology of the companion seems relatively undisturbed (see the inset in Figure 1) seems hard to explain if the interaction were responsible for the large disturbance in the main galaxy. Finally, even if this interaction were in some way significant, it would not explain why star formation in the inner parts of the main galaxy, which have not been affected dynamically, has shut down. So we conclude that NGC 1023A cannot be central to the question of how NGC 1023 was transformed into an S0 galaxy originally.

A more interesting scenario was presented by Burkert et al. (2005), who reported the discovery of a ring of diffuse star clusters in the disk of NGC 1023, which rotate but with large random motions, and suggested that NGC 1023 has undergone a head-on collision with a companion galaxy. Elmegreen (2007) showed that the star formation triggered by such an event will naturally lead to the formation of the kind of diffuse clusters observed in this galaxy. The maximum in the V/σ-profile in Figure 5 coincides with the ring of clusters, which suggests that the former was produced in the collision event as well. Note, however, that we do not observe a ring-like structure in the distribution of PNe (see Figure 4), which makes the connection somewhat speculative.

One other remaining plausible scenario is that the outer kinematics of NGC 1023 pre-date its transformation to an S0. If the progenitor spiral already had peculiar kinematics when it was stripped of its gas, then they would have remained imprinted in the final lenticular system. Similarly, if the parent galaxy in a minor merger has a constant velocity dispersion profile at large radii, rather than the declining profile usually assumed in simulations (e.g. Bournaud et al. 2005), than the end-product may well have a rising dispersion profile instead of a flat one. Very few spiral galaxies have had their stellar kinematics probed out to beyond three scale-lengths where the peculiarities begin, so we do not know how likely such a scenario might be. We do, however, already have some initial indications that random motions may be more prevalent in the outskirts of stellar discs: in their study of the PN kinematics of

M31, Merrett et al. (2006) found that outside two disc scale-lengths in this system the expected decline in stellar velocity dispersion with radius ceased, while Ciardullo et al. (2004) and Herrmann & Ciardullo (2005) found similar results for M33 and M83.

Ultimately, the conclusion here must be that even apparently simple-looking systems like S0s can be dynamically quite complex, presumably reflecting the complexities of the reality of galaxy evolution. Based on the single system presented in this study, we cannot make definitive statements about which processes are most important in the transformation of spiral galaxies into lenticulars. To disentangle the complexities in this transformation, we must not only look in detail at all the clues provided by each individual system, but we must also study significant numbers of both types of galaxies.

ACKNOWLEDGEMENTS

We would like to thank Andi Burkert for valuable comments. AJR was supported by the FONDAP Center for Astrophysics CONICYT 15010003 and by the National Science Foundation Grant AST-0507729. MRM is currently funded by an STFC Senior Fellowship. We thank the referee, Frederic Bournaud, for a thorough review and useful suggestions.

REFERENCES

Barbon R., Capaccioli M., 1975, A&A, 42, 103

Barway S., Kembhavi A., Wadadekar Y., Ravikumar C. D., Mayya Y. D., 2007, ApJ, 661, L37

Bedregal A. G., Aragón-Salamanca A., Merrifield M. R., 2006, MNRAS, 373, 1125

Begeman K., 1987, PhD thesis, Rijksuniversiteit Groningen

Begeman K. G., 1989, A&A, 223, 47

Bekki K., 1998, ApJ, 502, L133

Binney J., Tremaine S., 1987, Galactic dynamics. Princeton, NJ, Princeton University Press, 1987

Bournaud F., Combes F., Jog C. J., 2004, A&A, 418, L27

Bournaud F., Jog C. J., Combes F., 2005, A&A, 437, 69

Burkert A., Brodie J., Larsen S., 2005, ApJ, 628, 231

Capaccioli M., Lorenz H., Afanasjev V. L., 1986, A&A, 169, 54

Christlein D., Zabludoff A. I., 2004, ApJ, 616, 192

Ciardullo R., Durrell P. R., Laychak M. B., Herrmann K. A., Moody K., Jacoby G. H., Feldmeier J. J., 2004, ApJ, 614, 167

Couch W. J., Barger A. J., Smail I., Ellis R. S., Sharples R. M., 1998, ApJ, 497, 188

Debattista V. P., Corsini E. M., Aguerri J. A. L., 2002, MNRAS, 332, 65

Di Matteo P., Combes F., Melchior A. ., Semelin B., 2007, ArXiv e-prints: 0710.1293

Douglas N. G., Arnaboldi M., Freeman K. C., Kuijken K., Merrifield M. R., Romanowsky A. J., Taylor K., Capaccioli M., Axelrod T., Gilmozzi R., Hart J., Bloxham G., Jones D., 2002, PASP, 114, 1234

Douglas N. G., Napolitano N. R., Romanowsky A. J., Coccato L., Kuijken K., Merrifield M. R., Arnaboldi M., Gerhard O., Freeman K. C., Merrett H. R., Noordermeer E., Capaccioli M., 2007, ApJ, 664, 257

Dressler A., 1980, ApJ, 236, 351

Dressler A., Oemler A. J., Couch W. J., Smail I., Ellis R. S., Barger A., Butcher H., Poggianti B. M., Sharples R. M., 1997, ApJ, 490, 577

Elmegreen B. G., 2007, ArXiv e-prints: 0710.5788

Emsellem E., Cappellari M., Peletier R. F., McDermid R. M., Bacon R., Bureau M., Copin Y., Davies R. L., Krajnović D., Kuntschner H., Miller B. W., Tim de Zeeuw P., 2004, MNRAS, 352, 721

Herrmann K. A., Ciardullo R., 2005, in Szczerba R., Stasinska G., Gorny S. K., eds, Planetary Nebulae as Astronomical Tools Vol. 804 of American Institute of Physics Conference Series, Planetary Nebula Studies of Face-On Spiral Galaxies: Is the Disk Mass-to-Light Ratio Constant?. pp 341–344

Hubble E. P., 1926, ApJ, 64, 321

Hui X., Ford H. C., Ciardullo R., Jacoby G. H., 1993, ApJ, 414, 463

Laurikainen E., Salo H., Buta R., 2005, MNRAS, 362, 1319

Mathieu A., Merrifield M. R., Kuijken K., 2002, MNRAS, 330, 251

Merrett H. R., Merrifield M. R., Douglas N. G., Kuijken K., Romanowsky A. J., Napolitano N. R., Arnaboldi M., Capaccioli M., Freeman K. C., Gerhard O., Coccato L., Carter D., Evans N. W., Wilkinson M. I., Halliday C., Bridges T. J., 2006, MNRAS, 369, 120

Neistein E., Maoz D., Rix H.-W., Tonry J. L., 1999, AJ, 117, 2666

Noordermeer E., Verheijen M. A. W., 2007, ArXiv Astrophysics e-prints: astro-ph/0708.2822

Quilis V., Moore B., Bower R., 2000, Science, 288, 1617

Quinn P. J., Hernquist L., Fullagar D. P., 1993, ApJ, 403, 74

Sancisi R., van Woerden H., Davies R. D., Hart L., 1984, MNRAS, 210, 497

Seifert W., Scorza C., 1996, A&A, 310, 75

Simien F., Prugniel P., 1997, A&AS, 126, 519

Tonry J. L., Dressler A., Blakeslee J. P., Ajhar E. A., Fletcher A. B., Luppino G. A., Metzger M. R., Moore C. B., 2001, ApJ, 546, 681

Tully R. B., 1980, ApJ, 237, 390

Velázquez H., White S. D. M., 1999, MNRAS, 304, 254

Table 2. Catalogue of PNe in NGC 1023 and NGC 1023A.

ID	RA (2000)			Dec (2000)			$V_{\rm hel}$	notes	ID	RA (2000)			Dec (2000)			$V_{\rm hel}$	notes
PNS-EPN-	h	m	s	$^\circ$	$'$	$''$	km s^{-1}		PNS-EPN-	h	m	s	$^\circ$	$'$	$''$	km s^{-1}	
NGC 1023 1	2	39	55.92	39	3	33.2	730 ± 14		NGC 1023 65	2	40	18.09	39	4	50.2	466 ± 13	
NGC 1023 2	2	39	57.40	39	3	14.1	772 ± 13		NGC 1023 66	2	40	18.18	39	3	55.4	376 ± 16	
NGC 1023 3	2	39	59.24	39	4	28.3	446 ± 14		NGC 1023 67	2	40	18.19	39	3	42.3	386 ± 17	
NGC 1023 4	2	40	1.35	39	4	30.6	639 ± 13		NGC 1023 68	2	40	18.31	39	4	13.9	348 ± 14	
NGC 1023 5	2	40	1.71	39	2	55.7	510 ± 13		NGC 1023 69	2	40	18.35	39	3	58.7	461 ± 13	
NGC 1023 6	2	40	2.55	39	4	17.5	397 ± 13		NGC 1023 70	2	40	18.42	39	3	28.5	334 ± 13	
NGC 1023 7	2	40	2.60	39	3	56.0	675 ± 13		NGC 1023 71	2	40	19.22	39	5	59.3	898 ± 13	
NGC 1023 8	2	40	3.93	39	5	49.4	473 ± 14		NGC 1023 72	2	40	19.31	39	2	51.7	494 ± 14	
NGC 1023 9	2	40	6.13	39	3	38.8	550 ± 28		NGC 1023 73	2	40	19.39	39	3	52.2	366 ± 13	
NGC 1023 10	2	40	6.48	39	2	56.0	453 ± 13		NGC 1023 74	2	40	20.20	39	3	16.4	427 ± 13	
NGC 1023 11	2	40	6.53	39	4	24.2	740 ± 15		NGC 1023 75	2	40	20.35	39	5	1.0	485 ± 14	
NGC 1023 12	2	40	6.85	39	1	34.9	767 ± 13		NGC 1023 76	2	40	20.39	39	4	0.9	561 ± 18	
NGC 1023 13	2	40	6.99	39	4	4.5	410 ± 13		NGC 1023 77	2	40	20.40	39	3	15.2	444 ± 14	
NGC 1023 14	2	40	7.00	39	1	17.7	408 ± 14		NGC 1023 78	2	40	20.97	39	3	49.9	442 ± 13	
NGC 1023 15	2	40	7.09	39	3	57.3	701 ± 13		NGC 1023 79	2	40	21.11	39	3	47.5	442 ± 14	
NGC 1023 16	2	40	7.21	39	2	40.2	446 ± 13		NGC 1023 80	2	40	21.12	39	4	11.7	543 ± 13	
NGC 1023 17	2	40	7.46	39	2	4.8	790 ± 32		NGC 1023 81	2	40	21.22	39	3	8.3	535 ± 16	
NGC 1023 18	2	40	8.38	39	3	33.8	456 ± 16		NGC 1023 82	2	40	21.81	39	1	11.6	787 ± 18	
NGC 1023 19	2	40	8.46	39	3	43.0	548 ± 13		NGC 1023 83	2	40	21.85	39	5	9.1	619 ± 13	
NGC 1023 20	2	40	9.68	39	2	50.2	379 ± 13		NGC 1023 84	2	40	21.95	39	5	25.9	603 ± 13	
NGC 1023 21	2	40	9.77	39	3	10.2	385 ± 13		NGC 1023 85	2	40	22.26	39	2	31.7	606 ± 13	
NGC 1023 22	2	40	9.81	39	3	13.9	447 ± 13		NGC 1023 86	2	40	22.27	39	2	3.8	661 ± 15	
NGC 1023 23	2	40	10.23	39	3	36.8	733 ± 13	a	NGC 1023 87	2	40	22.28	39	2	51.2	537 ± 13	
NGC 1023 24	2	40	10.91	39	4	29.6	372 ± 13		NGC 1023 88	2	40	22.31	39	4	20.2	592 ± 13	
NGC 1023 25	2	40	11.07	39	3	53.3	489 ± 13		NGC 1023 89	2	40	22.32	39	4	29.5	586 ± 14	
NGC 1023 26	2	40	11.11	39	2	25.5	600 ± 14		NGC 1023 90	2	40	22.60	39	4	39.9	696 ± 13	
NGC 1023 27	2	40	11.40	39	2	23.8	587 ± 23		NGC 1023 91	2	40	22.64	39	4	13.9	485 ± 14	
NGC 1023 28	2	40	11.64	39	4	50.6	511 ± 13		NGC 1023 92	2	40	23.06	39	4	9.2	675 ± 14	
NGC 1023 29	2	40	11.84	39	3	49.4	465 ± 13		NGC 1023 93	2	40	23.51	39	3	26.8	599 ± 15	
NGC 1023 30	2	40	12.16	39	3	32.8	490 ± 13		NGC 1023 94	2	40	23.84	39	4	31.8	499 ± 13	
NGC 1023 31	2	40	12.32	39	3	44.0	350 ± 19		NGC 1023 95	2	40	24.05	39	2	47.4	582 ± 31	
NGC 1023 32	2	40	12.78	39	3	6.6	511 ± 24		NGC 1023 96	2	40	24.22	39	5	27.5	768 ± 13	
NGC 1023 33	2	40	12.89	39	3	7.5	523 ± 24		NGC 1023 97	2	40	24.41	39	3	15.2	742 ± 14	
NGC 1023 34	2	40	13.49	39	4	30.2	471 ± 13		NGC 1023 98	2	40	24.49	39	8	11.0	737 ± 14	
NGC 1023 35	2	40	13.52	39	3	58.6	447 ± 14		NGC 1023 99	2	40	25.05	39	4	47.8	738 ± 14	
NGC 1023 36	2	40	13.79	39	3	28.5	390 ± 14		NGC 1023 100	2	40	25.06	39	4	22.4	588 ± 14	
NGC 1023 37	2	40	14.12	39	5	45.2	566 ± 13		NGC 1023 101	2	40	25.24	39	4	7.8	512 ± 17	
NGC 1023 38	2	40	14.25	39	3	16.3	305 ± 16		NGC 1023 102	2	40	25.31	39	3	16.9	612 ± 14	
NGC 1023 39	2	40	14.57	39	4	36.0	479 ± 13		NGC 1023 103	2	40	25.33	39	4	20.9	571 ± 13	
NGC 1023 40	2	40	14.61	39	3	18.2	357 ± 13		NGC 1023 104	2	40	25.48	39	4	22.7	729 ± 14	
NGC 1023 41	2	40	14.65	39	3	54.5	371 ± 13		NGC 1023 105	2	40	25.59	39	4	53.2	745 ± 13	
NGC 1023 42	2	40	14.85	39	3	3.5	441 ± 13		NGC 1023 106	2	40	25.78	39	3	1.5	531 ± 14	
NGC 1023 43	2	40	14.90	39	4	16.0	898 ± 13	a	NGC 1023 107	2	40	25.80	39	3	32.0	534 ± 13	
NGC 1023 44	2	40	14.97	39	3	16.5	449 ± 13		NGC 1023 108	2	40	25.83	39	3	35.1	573 ± 16	
NGC 1023 45	2	40	15.11	39	3	45.0	516 ± 13		NGC 1023 109	2	40	25.94	39	3	9.6	591 ± 13	
NGC 1023 46	2	40	15.11	39	4	30.8	560 ± 13		NGC 1023 110	2	40	26.03	39	2	42.6	688 ± 13	
NGC 1023 47	2	40	15.25	39	3	9.1	372 ± 13		NGC 1023 111	2	40	26.05	39	4	30.6	672 ± 13	
NGC 1023 48	2	40	15.33	39	2	55.0	346 ± 13		NGC 1023 112	2	40	26.22	39	2	19.8	566 ± 13	
NGC 1023 49	2	40	16.03	39	3	0.6	486 ± 13		NGC 1023 113	2	40	26.26	39	2	33.6	662 ± 13	
NGC 1023 50	2	40	16.17	39	3	7.8	545 ± 13		NGC 1023 114	2	40	26.39	39	4	47.6	681 ± 13	
NGC 1023 51	2	40	16.31	39	4	22.8	440 ± 13		NGC 1023 115	2	40	26.82	39	3	17.4	691 ± 14	
NGC 1023 52	2	40	16.33	39	2	54.8	581 ± 13		NGC 1023 116	2	40	26.92	39	4	2.8	928 ± 13	
NGC 1023 53	2	40	16.35	39	2	38.8	775 ± 13		NGC 1023 117	2	40	27.01	39	3	46.0	740 ± 13	
NGC 1023 54	2	40	16.41	39	2	6.0	381 ± 16		NGC 1023 118	2	40	27.08	39	4	12.6	767 ± 13	
NGC 1023 55	2	40	16.49	39	4	57.3	474 ± 14		NGC 1023 119	2	40	27.12	39	3	51.0	854 ± 17	
NGC 1023 56	2	40	16.60	39	3	19.1	460 ± 13		NGC 1023 120	2	40	27.33	39	4	1.5	724 ± 13	
NGC 1023 57	2	40	16.86	39	2	19.4	570 ± 19		NGC 1023 121	2	40	27.35	39	4	8.4	801 ± 13	
NGC 1023 58	2	40	17.05	39	1	2.3	591 ± 13		NGC 1023 122	2	40	27.48	39	4	35.5	736 ± 13	
NGC 1023 59	2	40	17.17	39	3	0.3	467 ± 14		NGC 1023 123	2	40	27.51	39	4	39.0	794 ± 13	
NGC 1023 60	2	40	17.30	39	4	3.0	389 ± 14		NGC 1023 124	2	40	27.52	39	3	10.9	625 ± 18	
NGC 1023 61	2	40	17.36	39	4	11.0	540 ± 13		NGC 1023 125	2	40	27.60	39	4	15.5	846 ± 13	
NGC 1023 62	2	40	17.56	39	3	47.3	635 ± 13		NGC 1023 126	2	40	28.11	39	4	6.0	802 ± 15	
NGC 1023 63	2	40	17.56	39	4	9.4	338 ± 14		NGC 1023 127	2	40	28.18	39	2	3.1	410 ± 14	
NGC 1023 64	2	40	17.95	39	4	10.0	495 ± 13		NGC 1023 128	2	40	28.65	39	3	54.8	773 ± 13	

Table 2 – *continued* Catalogue of PNe in NGC 1023 and NGC 1023A.

ID	RA (2000)			Dec (2000)			V_{hel}	notes	ID	RA (2000)			Dec (2000)			V_{hel}	notes
PNS-EPN-	*h*	*m*	*s*	°	′	″	km s^{-1}		PNS-EPN-	*h*	*m*	*s*	°	′	″	km s^{-1}	
NGC 1023 129	2	40	28.77	39	3	47.1	684 ± 13		NGC 1023 167	2	40	35.70	39	3	45.2	753 ± 13	
NGC 1023 130	2	40	28.87	39	4	0.2	846 ± 13		NGC 1023 168	2	40	35.74	39	3	26.3	830 ± 13	c
NGC 1023 131	2	40	29.07	39	3	22.5	859 ± 13		NGC 1023 169	2	40	35.76	39	3	32.8	777 ± 14	c
NGC 1023 132	2	40	29.20	39	4	35.7	762 ± 13		NGC 1023 170	2	40	36.76	39	3	14.6	723 ± 13	c
NGC 1023 133	2	40	29.31	39	3	42.2	726 ± 13		NGC 1023 171	2	40	36.83	39	3	46.9	767 ± 13	c
NGC 1023 134	2	40	29.38	39	4	17.0	725 ± 16		NGC 1023 172	2	40	36.86	39	2	52.3	741 ± 13	c
NGC 1023 135	2	40	29.39	39	4	21.9	859 ± 14		NGC 1023 173	2	40	37.07	39	3	3.6	771 ± 14	c
NGC 1023 136	2	40	29.43	39	3	28.4	745 ± 14		NGC 1023 174	2	40	37.44	39	3	23.7	732 ± 13	c
NGC 1023 137	2	40	29.49	39	3	5.4	765 ± 13		NGC 1023 175	2	40	37.55	39	3	43.2	722 ± 13	c
NGC 1023 138	2	40	29.53	39	4	45.7	683 ± 14		NGC 1023 176	2	40	37.79	39	3	41.8	828 ± 13	c
NGC 1023 139	2	40	29.65	39	3	58.8	649 ± 13		NGC 1023 177	2	40	37.87	39	2	25.6	750 ± 13	c
NGC 1023 140	2	40	29.72	39	2	23.8	741 ± 13		NGC 1023 178	2	40	38.01	39	3	1.5	744 ± 13	c
NGC 1023 141	2	40	30.06	39	4	0.0	833 ± 13		NGC 1023 179	2	40	38.13	39	3	35.5	808 ± 13	c
NGC 1023 142	2	40	30.25	39	3	51.4	835 ± 13		NGC 1023 180	2	40	38.16	39	4	14.2	748 ± 13	
NGC 1023 143	2	40	30.44	39	4	3.8	661 ± 17		NGC 1023 181	2	40	38.79	39	3	34.8	848 ± 13	c
NGC 1023 144	2	40	30.58	39	5	54.7	450 ± 13		NGC 1023 182	2	40	39.41	39	4	49.7	750 ± 13	
NGC 1023 145	2	40	30.60	39	3	39.0	855 ± 13		NGC 1023 183	2	40	39.91	39	4	12.1	822 ± 13	c
NGC 1023 146	2	40	30.74	39	3	20.3	812 ± 13		NGC 1023 184	2	40	40.04	39	3	45.9	736 ± 13	c
NGC 1023 147	2	40	31.08	39	4	38.2	868 ± 13		NGC 1023 185	2	40	40.24	39	5	29.0	716 ± 13	
NGC 1023 148	2	40	31.29	39	3	27.2	809 ± 13		NGC 1023 186	2	40	40.52	39	7	1.3	664 ± 13	
NGC 1023 149	2	40	31.76	39	3	34.2	766 ± 14		NGC 1023 187	2	40	40.71	39	3	50.4	781 ± 13	c
NGC 1023 150	2	40	31.77	39	3	41.1	874 ± 13		NGC 1023 188	2	40	40.74	39	5	51.1	769 ± 13	
NGC 1023 151	2	40	32.48	39	3	54.6	772 ± 14		NGC 1023 189	2	40	40.78	39	4	38.4	787 ± 13	
NGC 1023 152	2	40	32.77	39	4	11.8	856 ± 13		NGC 1023 190	2	40	40.85	39	6	33.6	700 ± 35	
NGC 1023 153	2	40	32.85	39	4	49.2	745 ± 13		NGC 1023 191	2	40	41.09	39	4	21.1	419 ± 13	a
NGC 1023 154	2	40	33.21	39	3	37.7	776 ± 13		NGC 1023 192	2	40	41.41	39	5	17.1	717 ± 14	
NGC 1023 155	2	40	33.30	39	3	29.8	780 ± 13		NGC 1023 193	2	40	41.67	39	8	17.0	610 ± 13	
NGC 1023 156	2	40	33.35	39	3	47.0	823 ± 16		NGC 1023 194	2	40	41.89	39	1	28.3	757 ± 13	
NGC 1023 157	2	40	33.39	39	3	10.6	786 ± 14		NGC 1023 195	2	40	42.40	39	3	43.5	748 ± 13	c
NGC 1023 158	2	40	33.68	39	4	46.5	728 ± 13		NGC 1023 196	2	40	42.54	39	4	25.3	813 ± 16	
NGC 1023 159	2	40	33.68	39	3	24.7	765 ± 15		NGC 1023 197	2	40	43.07	39	2	38.0	741 ± 13	
NGC 1023 160	2	40	33.76	39	3	10.5	810 ± 14	c	NGC 1023 198	2	40	43.09	39	4	4.8	658 ± 13	
NGC 1023 161	2	40	34.04	39	4	35.2	618 ± 13		NGC 1023 199	2	40	44.40	39	3	43.5	785 ± 13	
NGC 1023 162	2	40	34.40	39	2	37.0	755 ± 14	c	NGC 1023 200	2	40	44.73	39	2	7.0	1703 ± 13	b
NGC 1023 163	2	40	34.50	39	4	2.9	813 ± 13		NGC 1023 201	2	40	44.77	39	4	7.6	545 ± 13	
NGC 1023 164	2	40	34.68	39	3	57.4	832 ± 17		NGC 1023 202	2	40	46.40	39	1	3.4	452 ± 13	
NGC 1023 165	2	40	34.83	39	3	43.4	812 ± 13		NGC 1023 203	2	40	47.71	39	6	5.1	804 ± 13	
NGC 1023 166	2	40	35.53	39	3	12.3	745 ± 13	c	NGC 1023 204	2	40	48.98	39	3	58.8	734 ± 13	

explanation of the notes:

a $> 3\sigma$ outlier in the tilted ring analysis

b Discrepant velocity; unbound to system

c Object statistically more likely to belong to companion NGC 1023A than to main galaxy NGC 1023.